www.acsnano.org

# Facile Synthesis of Silicone Oil-Based Ferrofluid: Toward Smart Materials and Soft Robots

Leilei Chen, Hengao Yu, Jilan Yang, Jinzhuo Shi, Chun-he Li, Zijie Qu, and Wendong Wang\*



Downloaded via SHANGHAI JIAO TONG UNIV on August 6, 2025 at 12:37:29 (UTC). See https://pubs.acs.org/sharingguidelines for options on how to legitimately share published articles.

Cite This: ACS Nano 2025, 19, 8904-8915



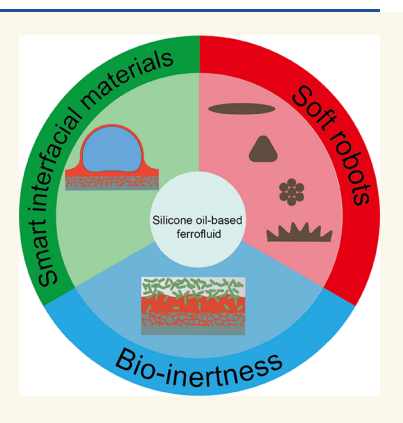
**ACCESS** 

Metrics & More

Article Recommendations

Supporting Information

ABSTRACT: Ferrofluids are stable colloidal dispersions of magnetic nanoparticles in carrier liquids. Their combination of magnetic and fluidic characteristics not only inspires fundamental inquiries into forms and functions of matter but also enables diverse applications ranging from sealants and coolants in mechanical devices to active components in smart materials and soft robots. Spurred by such fundamental and applied interests, a growing need for easy-to-synthesize, high-quality ferrofluid exists. Here, we report the facile synthesis and comprehensive characterization of a silicone oil-based ferrofluid that displays the characteristic surface instability of high-quality ferrofluids and demonstrate its functions in smart interfacial materials and soft robots. Silicone's chemical immiscibility with polar solvents and its biological inertness, when coupled with magnetic responsiveness and fluidic deformability, enable the manipulation of solid particles, gas bubbles, simple and complex liquids, as well as micro-organisms. We envision that the silicone oil-based ferrofluid will find applications in diverse areas, including magnetic digital microfluidics, multifunctional materials, and small-scale robotics.



KEYWORDS: magnetic materials, ferrofluid, self-assembly, programmable materials, smart materials, soft robots

# **INTRODUCTION**

Ferrofluids are stable colloidal dispersions of magnetic nanoparticles in carrier liquids. <sup>1-5</sup> The nanoparticles are about 10 nm in size and are commonly composed of magnetite (Fe<sub>3</sub>O<sub>4</sub>), maghemite (Fe<sub>2</sub>O<sub>3</sub>), or cobalt ferrite (CoO·Fe<sub>2</sub>O<sub>3</sub>). They can be stabilized against agglomeration by surface charges, as in many water-based ferrofluids, or by a layer of surfactant or polymeric coatings, as in oil-based ferrofluids. (Ferrofluids are not to be confused with magnetorheological fluids,6 which consist of micron-sized particles and thus have very different properties and functions.) Ferrofluids have been used as sealants in switches and pumps, coolants in loudspeakers, delivery agents, and contrast agents in medical imaging. 2-5,7,8 Recently, ferrofluids have been used as active components in multifunctional interfacial materials, <sup>9-11</sup> droplet-based microfluidic systems, <sup>12-14</sup> and soft robots. <sup>15-25</sup> As a result, their potential applications have expanded into emerging areas such as programmable matter<sup>26</sup> and intelligent matter.

Many unique properties of ferrofluids stem from the synergy between the magnetic particles and their carrier liquids; therefore, changing the chemical composition of the carrier liquid of a ferrofluid significantly alters its properties. The most common carrier liquids are water and hydrocarbon oils. Many of these water- or hydrocarbon-oil-based ferrofluids are commercially available and have been used in recent demonstrations of

ferrofluid-based robots. 15-25 However, their miscibility with water, common organic solvents, such as ethanol, and complex biofluids, such as blood, poses risks of sample contamination and degradation. Fluorocarbon-based ferrofluids<sup>9,28</sup> can overcome the miscibility challenge because of their chemical and biological inertness, but using per- and poly-fluoroalkyl substances brings additional safety concerns because of their long-term accumulation in the environment.<sup>29</sup> Silicone oils, or more technically called polysiloxane liquids, are also chemically and biologically inert. They are considered superior to hydrocarbon oils in many properties, such as high thermal stability, small dependence of viscosity on temperature, and low surface tension. 30-33 Their superior properties have enabled applications including additive manufacturing,<sup>34</sup> slippery coatings,<sup>35,36</sup> pharmaceutical storage,<sup>37,38</sup> and clinical operations.<sup>39,40</sup> It is therefore expected that silicone oil-based ferrofluids would have similarly diverse applications.

Received: November 20, 2024 Revised: February 21, 2025 Accepted: February 24, 2025 Published: March 3, 2025





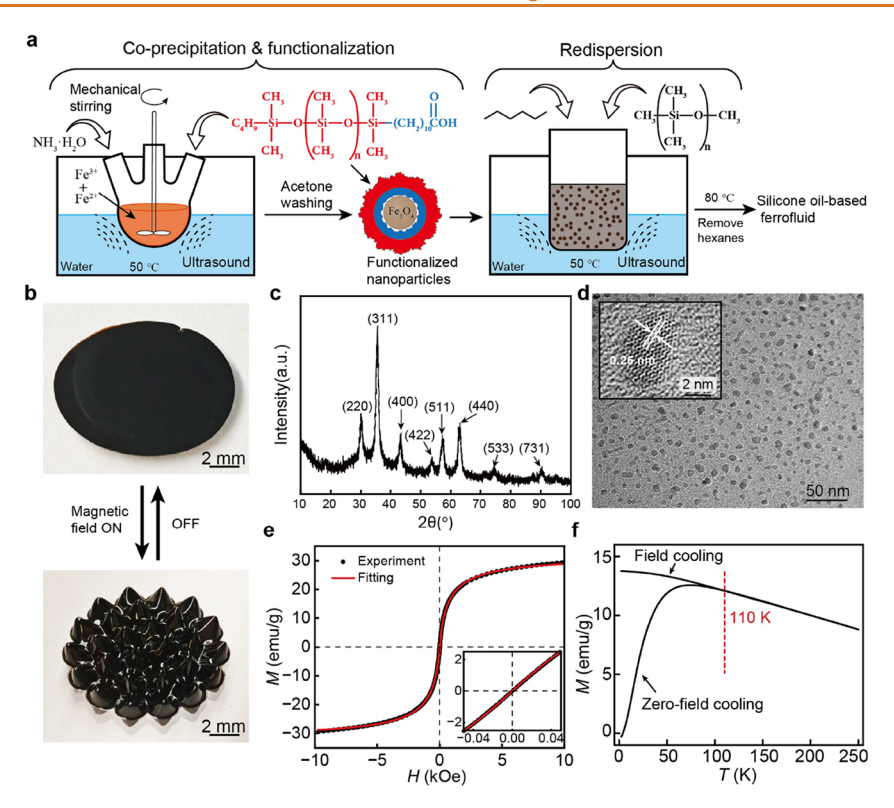


Figure 1. Structural characterizations and magnetic properties of silicone oil-based ferrofluid. (a) Scheme of the two-step synthesis. (b) Photo of the surface instability of the as-synthesized silicone oil-based ferrofluid. (c) X-ray diffractogram of the functionalized  $Fe_3O_4$  nanoparticles. The peaks are labeled according to magnetite ICSD #26410. (d) Representative transmission electron microscopy image showing the functionalized nanoparticles. The inset shows the crystal lattice. (e) Plot of the ferrofluid magnetization M versus the applied field H. The inset magnifies the region from -40 to 40 Oe. The M-H curve shows no hysteresis, in agreement with the superparamagnetism of the nanoparticles. The red curve is the fitting of the Langevin function. (f) Plot of zero-field cooling and field-cooling ferrofluid magnetizations M versus temperature T. The dashed red vertical line at 110 K indicates the blocking temperature of the ferromagnetism—superparamagnetism transition.

Existing silicone oil-based ferrofluids, 41-50 however, have not fully realized these potentials. The challenge is mostly due to the difficulty in uniformly and stably dispersing magnetic nanoparticles in silicone oils (Table S1). Commercial ferrofluids are mostly water- or hydrocarbon-based ferrofluids; silicone oilbased ferrofluids are rare, and their qualities are uncertain (Table S2). Early patents explored using single-end functionalized polysiloxane as surfactants<sup>41</sup> but found it difficult to anchor these surfactants on nanoparticles. 42 This same strategy was adopted in our previous report<sup>9</sup> and the report of Zhou et al.,<sup>49</sup> but no surface instabilities were observed. Another strategy was to use hydrocarbon surfactants, 48,50 but this strategy created potential solubility issues with many other hydrocarbon fluids. Yet another strategy was to use siloxane-based surfactants with multiple anchor points, 42–44,46,47 but it tends to agglomerate nanoparticles and induce sedimentation. Hence, the potential of silicone oil-based ferrofluids as a model system for fundamental studies on ferrohydrodynamics or as active components in soft robots, smart materials, or systems has not been fully realized.

Here we report the facile synthesis of a silicone oil-based ferrofluid with high saturation magnetization and demonstrate its wide range of interfacial and robotic functions. Specifically, we employ sonication to assist the bonding between the monocarboxyl-terminated poly(dimethylsiloxane) and iron oxide nanoparticles under mild synthesis conditions. The resulting ferrofluid possesses saturation magnetization close to  $30 \, \text{emu/g} \ (\sim\!490 \, \text{G})$  and displays the surface instability characteristic of a high-quality ferrofluid. We characterize the ferrofluid's rheological and mechanical properties and its

chemical compatibilities with representative polar and nonpolar solutions/solvents, as well as reactive solutions. We further demonstrate its interfacial functions in droplet-based microfluidic systems on slippery-liquid-infused porous surfaces (SLIPS) and ferrofluid-infused porous surfaces (FLIPS) and illustrate its bioinert properties in bacteria, algae, and mammalian cell cultures. Moreover, the dynamic topographical response in FLIPS provides additional antibiofouling properties. Finally, we demonstrate the potential of ferrofluid-based robots using ferrofluid droplets. We envision that our silicone oil-based ferrofluid will find applications in magnetic digital microfluidics for chemical and biomedical testing, in multifunctional materials for antifouling and protective coatings, and in microrobots for targeted delivery and minimally invasive surgery.

## **RESULTS AND DISCUSSION**

Synthesis, Structure, and Magnetic Properties of Silicone Oil-Based Ferrofluid. The silicone oil-based ferrofluid was synthesized via ultrasound-assisted chemical coprecipitation, functionalization, and redispersion of iron oxide nanoparticles (Figure 1a). First, an acidic solution of divalent and trivalent iron cations was mixed with an ammonia solution to form iron oxide nanoparticles. Toward this mixture, monocarboxyldecyl-terminated polydimethylsiloxane (PDMS- $C_{10}COOH$ ) was added under continuous mechanical stirring and ultrasonication. In basic aqueous solutions, deprotonated carboxyl groups are bidentate ligands and form strong coordinate bonds with iron cations, thereby anchoring PDMS- $C_{10}COO^-$  to the nanoparticle surfaces. As a result, the

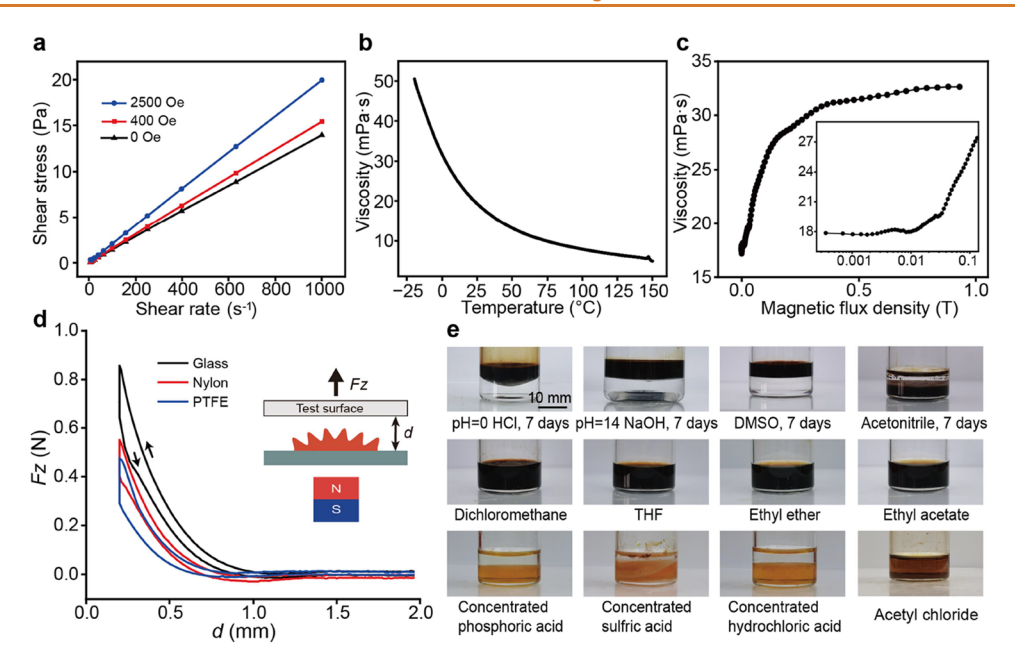


Figure 2. (a) Plot of shear stress versus shear rate of the as-synthesized ferrofluid under three different magnetic fields. (b) Plot of viscosity versus temperature at a constant shear rate of  $100 \text{ s}^{-1}$ . (c) Plot of viscosity versus magnetic flux density at a constant shear rate of  $500 \text{ s}^{-1}$ . The inset shows the data points in the low field region on a log scale. (d) Plot of vertical force versus separation distance for three test surfaces: glass, nylon, and PTFE. (e) Photos of chemical compatibility tests. The first row shows immiscible solutions and solvents. The second row shows miscible solvents. The third row shows reactive solutions and solvents.

functionalized nanoparticles are surrounded by an inner layer of carbon chains and an outer layer of PDMS groups. Then, the functionalized nanoparticles were washed with acetone and redispersed in n-hexane. Any remaining acetone and ammonia were removed by ultrasonication at 50 °C. Finally, dimethylsilicone oil (10 mPa·s) was added to the dispersion, and n-hexane was removed by raising the water bath temperature to 80 °C to obtain silicone oil-based ferrofluid. The quality of the final product was readily assessed by observation of the characteristic surface instability under a strong permanent magnet (Figure 1b).

Our previous synthesis used PDMS- $C_{10}$ COOH as the surfactant, but it did not produce a ferrofluid that displays surface instability. Our current synthesis improves upon the previous synthesis in the following three aspects: (1) we employ ultrasonication to increase reaction rates and shorten the total duration of the synthesis from 2 days to  $\sim$ 2 h; (2) we replace toluene with more volatile hexane in the dispersion step, thereby removing the need for the last step of heating in an oil bath; (3) we identify that the PDMS oils of low molecular weight are better than PDMS oils of high molecular weight in synthesizing high-quality ferrofluid. We comment on these three aspects below.

First, we performed control experiments to selectively turn off ultrasonication in each of the two steps in the synthesis, and the results show that ultrasonication in the coprecipitation and functionalization step is critical to the quality of the ferrofluid (Figure S1). Research in sonochemistry has shown that ultrasounds create cavities with sizes of  $\sim 1~\mu m$  and lifetimes of  $\sim 1~ns.^{51-53}$  In the low-frequency range of 20–100 kHz, mechanical effects, such as the shock waves and shear forces generated by the collapses of cavities, dominate, whereas in the high-frequency range of 100 kHz to 10 MHz, chemical effects, such as the formation of free radical species, dominate. The measured ultrasound frequency in our ultrasonication vessel is  $\sim 30~kHz$  at a power of  $\sim 0.7~W/cm^2$ , which is in the low-

frequency range. Moreover, the proton magnetic resonance spectra (Figure S2) and gel permeation chromatograms (Figure S3) of  $C_4$ -PDMS- $C_{10}$ COOH before and after ultrasonication treatment show little or no difference. Both results suggest the dominance of the mechanical effect of ultrasonication in our synthesis. Specifically, we surmise that (1) the ultrasonication increases the chances (per unit time) of surfactants' carboxylic acid groups interacting with nanoparticles' surface hydroxyl groups by rapidly reconfiguring the conformation of PDMS- $C_{10}$ COOH and that (2) it facilitates the condensation reaction between carboxylic acid and hydroxyl groups by providing extra energy to activate these groups, either in the form of kinetic energy released during the collapses of cavities or in the form of thermal energy.

Second, toluene was used in the dispersion step in our previous synthesis<sup>9</sup> because it is a good solvent for PDMS.<sup>54</sup> It can unfold the polymeric chains of PDMS groups in the outer layer of the functionalized nanoparticles and facilitate the interaction between these anchored PDMS groups and the chains of PDMS oils in the final dispersion. We hypothesized that other good solvents<sup>54</sup> of PDMS can achieve a similar effect. Indeed, *n*-hexane can redisperse the functionalized nanoparticles in PDMS oils. The boiling point of *n*-hexane (69 °C) is lower than that of toluene (110 °C) and can be easily removed by heating in the same ultrasonication water bath. Thus, the heating step in an oil bath is removed.

Third, low-molecular-weight PDMS oils are better than their high-molecular-weight counterparts because their contributions to the mixing entropy  $\Delta S_{\rm mix}$ , are higher. According to Flory–Huggins theory of polymer solubility (Supplementary Section S1), a polymer's contribution to the mixing entropy of polymeric solution is inversely proportional to its molecular weight or its degree of polymerization. Higher mixing entropy gives a lower mixing free energy and hence favors mixing. Control experiments performed with PDMS oil of 100 mPa·s did not produce a ferrofluid that displays surface instability

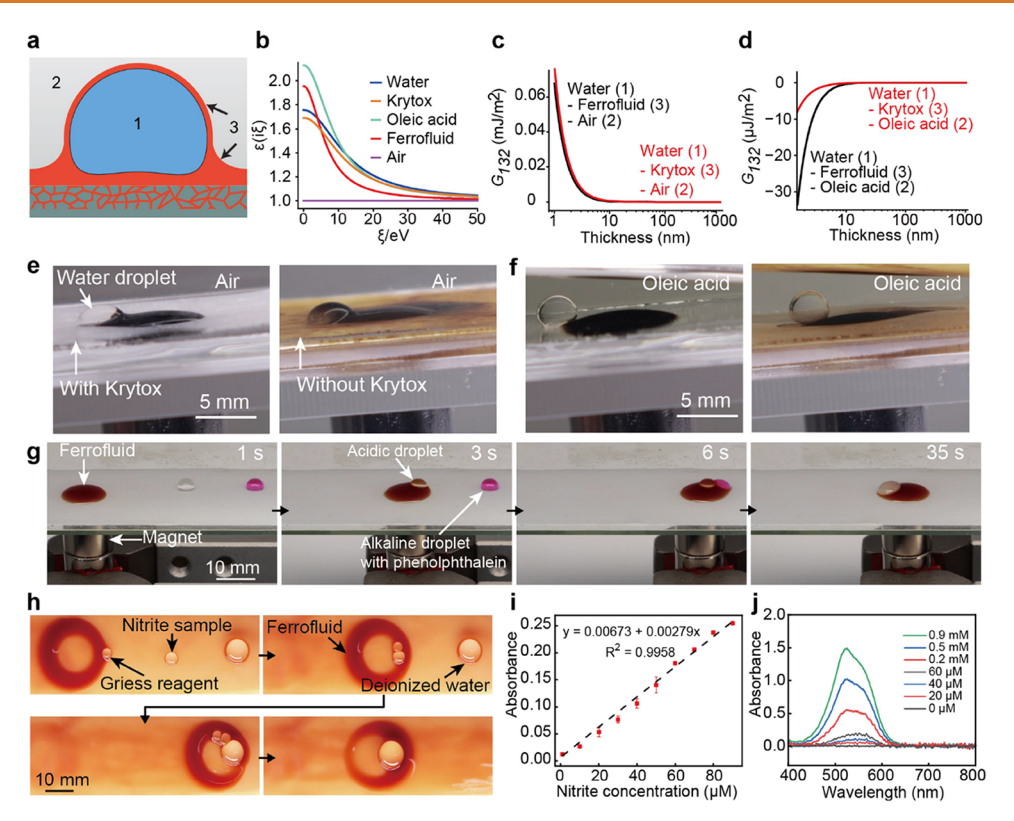


Figure 3. Interfacial properties and functions for droplet microfluidic platforms based on silicone oil-based ferrofluids. (a) Scheme of a wrapping layer: a droplet of fluid 1 (blue) is wrapped around by a thin film of fluid 3 (brown) in fluid 2 (gray). (b) Plots of dielectric coefficients  $\varepsilon$  versus frequency  $\xi$  (in unit of eV) for liquids used in our experiments. (c) Plots of Casimir–Lifshitz energy per unit area  $G_{132}$  versus the thickness of a wrapping layer. The configuration is a water droplet (1) wrapped by ferrofluid or hydrocarbon oil (3) in air (2). The numbers correspond to the configurations in panel a. Energy decreases with increasing thin film thickness, indicating stable thin films. (d) Plots of the Casimir–Lifshitz energy per unit area  $G_{132}$  versus the thickness of a wrapping layer. The configuration is a water droplet (1) wrapped by ferrofluid or hydrocarbon oil (3) in oleic acid (2). Energy decreases with decreasing thin film thickness, indicating unstable thin films. (e) Photos of water droplets held by magnets on SLIPS (left) and FLIPS (right) in air. (f) Photos showing the absence of a wrapping layer when oleic acid is added to replace air. (g) Demonstration of a ferrofluid droplet moving other droplets to perform an acid—based reaction on SLIPS. (h) Demonstration of a ferrofluid ring enclosing other droplets to perform a Griess test reaction on FLIPS. (i) Plot showing the linear dependence of absorbance on nitrite concentrations in the range of 1–100  $\mu$ M for the Griess test. (j) Selected absorption spectra of the Griess test.

(Figure S1e,f). The average molecular weights of PDMS oils of 10 and 100 mPa·s are 1800 and 5800 g/mol, respectively. Replacing PDMS oil of 100 mPa·s with PDMS oil of 10 mPa·s increases the oil's contribution to the mixing entropy by a factor of ~3, thereby creating a more stable solution. Indeed, the ferrofluid synthesized with PDMS oil of 10 mPa·s remained stable under strong magnetic field gradients for at least a month (Figure S4).

Figure 1c—f shows the crystalline structure of the iron oxide nanoparticles and the magnetic properties of the silicone oilbased ferrofluid. The X-ray diffraction (XRD) pattern shows that the nanoparticles are composed of magnetite Fe<sub>3</sub>O<sub>4</sub>, with the typical inverse spinel cubic structure (Figure 1c). No other phases of iron oxide were observed. The size of the nanoparticles obtained by transmission electron microscopy (TEM) is 6.0  $\pm$ 1.4 nm (Figures 1d and S5). The inset in Figure 1d shows the crystal lattice of a typical nanoparticle with a lattice spacing of 0.25 nm, corresponding to the (311) plane. The small sizes of the nanoparticles are consistent with their superparamagnetic properties. The curve of the ferrofluid magnetization M versus the magnetic field H was measured on a vibrating sample magnetometer at room temperature, and it shows no hysteresis (Figure 1e). Under the assumption of a log-normal distribution of particle sizes,  $^{56}$  the fitting of the M-H curve with the

Langevin function (Supplementary Section S2) gives a particle size of  $5.8 \pm 2.4$  nm, comparable with the size observed in TEM. The volume fraction of magnetite nanoparticles in the ferrofluid is about ~30%, estimated by dividing the saturation magnetization  $M_{\rm s} \sim 30$  emu/g of the ferrofluid by the bulk magnetization of magnetite  $M_{\rm b} \sim 98$  emu/g. The plot of zero-field-cooling and field-cooling magnetizations M versus temperature T indicates that the blocking transition temperature from ferromagnetism to superparamagnetism is about 110 K (Figure 1f), well below room temperature.

Rheological, Mechanical Properties, and Chemical Compatibilities. To understand comprehensively the behaviors of the silicone oil-based ferrofluid for applications, we characterize its rheological properties, mechanical properties, and chemical compatibilities (Figure 2). The rheological properties of the ferrofluid depend strongly on magnetic fields and temperature. The ferrofluid shows the behavior of a Newtonian fluid, with a linear relation between shear stress and shear rate up to 1000 s<sup>-1</sup> (Figure 2a). Its viscosity increases as the temperature decreases (Figure 2b); the rate of decrease is slower than that of water-based or hydrocarbon oil-based ferrofluids. Thus, the silicone oil-based ferrofluid keeps its viscosity within the same order of magnitude over a wide temperature range, allowing it to be used in high and low

Table 1. Spreading Coefficients for Ferrofluid/Krytox on Water Droplets in Air/Oleic Acid

| interface 1–2 $(\gamma_{12} [mN/m])$ | interface $3-1 (\gamma_{31} [mN/m])$ | interface $3-2 (\gamma_{32} [mN/m])$ | Spreading coefficient, $S = \gamma_{12} - (\gamma_{31} + \gamma_{32}) \text{ [mN/m]}$ | agreement with experiments |
|--------------------------------------|--------------------------------------|--------------------------------------|---|----------------------------|
| water-air (72)                       | ferrofluid-water (36.4)              | ferrofluid-air (21.0)                | 14.6  | yes                        |
| water-oleic acid (13.9)              | ferrofluid-water (36.4)              | ferrofluid—oleic acid (0.9)          | -23.4   | yes                        |
| water-air (72)                       | krytox-water (53.7)                  | Krytox-air (15.4)                    | 2.9   | yes                        |
| water-oleic acid (13.9)              | krytox-water (53.7)                  | Krytox-oleic acid (10.6)             | -50.4   | yes                        |

temperatures where other types of ferrofluids might fail. Its viscosity at room temperature increases as the magnetic field increases and plateaus at  $\sim 33$  mPa·s (Figure 2c); the shape of the curve resembles the shape of the magnetization curve, suggesting the dominant role of magnetization in increasing the effective viscosity. It suggests that the magnetic field can be used as a means of tuning the effective viscosity of the ferrofluid, which is potentially valuable in applications where a change in viscosity is required.

The silicone oil-based ferrofluid has a relatively low surface tension of 21 mN/m (Figure S6a). Thus, it wets many highenergy surfaces, such as glass and metals, and partially wets lowenergy surfaces, such as plastics. To investigate the effect of wetting on the ferrofluid's mechanical properties, we measured the forces between a ferrofluid droplet under a magnetic field and three test surfaces by first bringing the test surface down to 200  $\mu$ m above the bottom glass surface and retreating the test surface up (Figure 2d). The surface energies of the three test surfaces are ~200-500 mN/m for glass, ~46 mN/m for nylon, and ~18 mN/m for polytetrafluoroethylene (PTFE). Figure 2d shows that during both compression and extension, the upward forces increase with increasing surface energies of the test surfaces. We surmise that this effect is due to increasing interfacial interactions between the ferrofluid and the test surfaces, which suggests a way to tune mechanical functions using wetting properties in potential applications.

The chemical inertness of silicone oil suggests that the silicone oil-based ferrofluids should also be chemically inert. However, the presence of iron oxide nanoparticles, although surface functionalized, can be chemically active. We test the chemical compatibility of the silicone oil-based ferrofluid in three sets of representative solutions and solvents (Figure 2e). The first row shows the silicone oil-based ferrofluid with immiscible solutions and solvents after 7 days: aqueous solutions of pH = 0 and pH = 014, dimethyl sulfoxide (DMSO), and acetonitrile; the second row shows it with miscible solvents: dichloromethane, tetrahydrofuran (THF), ethyl ether, and ethyl acetate; the third row shows it with reactive solutions and solvents: concentrated phosphoric acid, concentrated sulfuric acid, concentrated hydrochloric acid, and acetyl chloride. These chemical compatibility tests suggest that the silicone oil-based ferrofluid is immiscible with more polar solvents and miscible with less polar solvents, but the presence of iron oxide makes it reactive with strong acids and corrosive compounds. These tests offer a guide for selecting materials in the applications of silicone-oil-based ferrofluids in smart materials and soft robots.

Smart Interfacial Materials Based on Silicone Oil-Based Ferrofluids. The chemical compatibilities of silicone oil-based ferrofluid enable its use on slippery liquid-infused porous surfaces (SLIPS)<sup>57,58</sup> or in ferrofluid-containing liquid-infused porous surfaces (FLIPS).<sup>9</sup> These smart surfaces can be designed to repel or manipulate various simple and complex liquids, solids, and biological soft materials. In particular, using ferrofluid to manipulate droplets on FLIPS or SLIPS provides a

new strategy for constructing magnetic digital microfluidic systems. 11 For these potential applications, understanding the fundamental interactions between the droplets and the underlying lubricating liquid serves as the foundation for the practical exploration of functions. One well-known phenomenon that reveals such fundamental interactions is the formation of a wrapping layer of lubricating liquid around a droplet (Figure 3a). Our new silicone oil-based ferrofluid allows easy visualization of the wrapping layer and displays qualitatively similar behaviors as the fluorocarbon-based ferrofluid in our previous report, but detailed quantitative analysis reveals new additional insights. Replacing fluorocarbon-based ferrofluids with our new ferrofluids in bioinspired interfacial materials will alleviate environmental concerns about fluorocarbons without sacrificing functions; thus, our new ferrofluids represent a more environmentally friendly alternative. This section will start with an investigation of the formation of wrapping layers and then demonstrate droplet manipulations on SLIPS and FLIPS as potential applications in magnetic digital microfluidics.

The formation of a wrapping layer is generally explained by the spreading coefficient,  $S = \gamma_{12} - (\gamma_{13} + \gamma_{23})$ , where  $\gamma_{ij}$ represents the interfacial tension between fluid i and fluid j, and fluids 1-3 represent the droplet, the surrounding fluid, and the fluid of the wrapping layer, respectively (Figure 3a). 59-61 An alternative approach based on the calculation of long-range van der Waals interactions, 62 also called Casimir-Lifshitz interactions, 63 was shown to give more accurate predictions for the formation of wrapping layers around water droplets on FLIPS.<sup>9</sup> For nonpolar liquids, such as silicone oils and fluorinated oils, van der Waals forces are the dominant contributions to surface tensions, so the two approaches should, in theory, yield the same results. In practice, however, trace amounts of impurities, such as dust organic particles in the air or small molecule plasticizers in plastic syringes and tubing, can significantly change the interfacial tension between water and a nonpolar fluid, thereby introducing errors large enough to alter the signs of spreading coefficients.

Here, we calculate both the spreading coefficients (Table 1) and the Casimir–Lifshitz interactions (Figure 3b–d) using the physical properties of the liquids (Tables S3 and S4) and compare these theoretical predictions with experimental results (Figure 3e–f and Movie S1). In our calculations and experiments, the droplet phase (fluid 1) is water; the surrounding fluid (fluid 2) is air or oleic acid; and the liquid of the wrapping layer (fluid 3) is silicone oil-based ferrofluid or fluorinated oil Krytox GPL100.

The calculation of spreading coefficients (Table 1) is straightforward when all the interfacial tensions are known (Table S4 and Figure S6, Supplementary Section S3). The results agree with the experimental observations. We make two comments. First, the large negative values of S in situations where oleic acid is the surrounding fluid are mostly due to the small interfacial tension between oleic acid and water (~14 mN/m). Oleic acid, being surface-active itself, has eliminated the

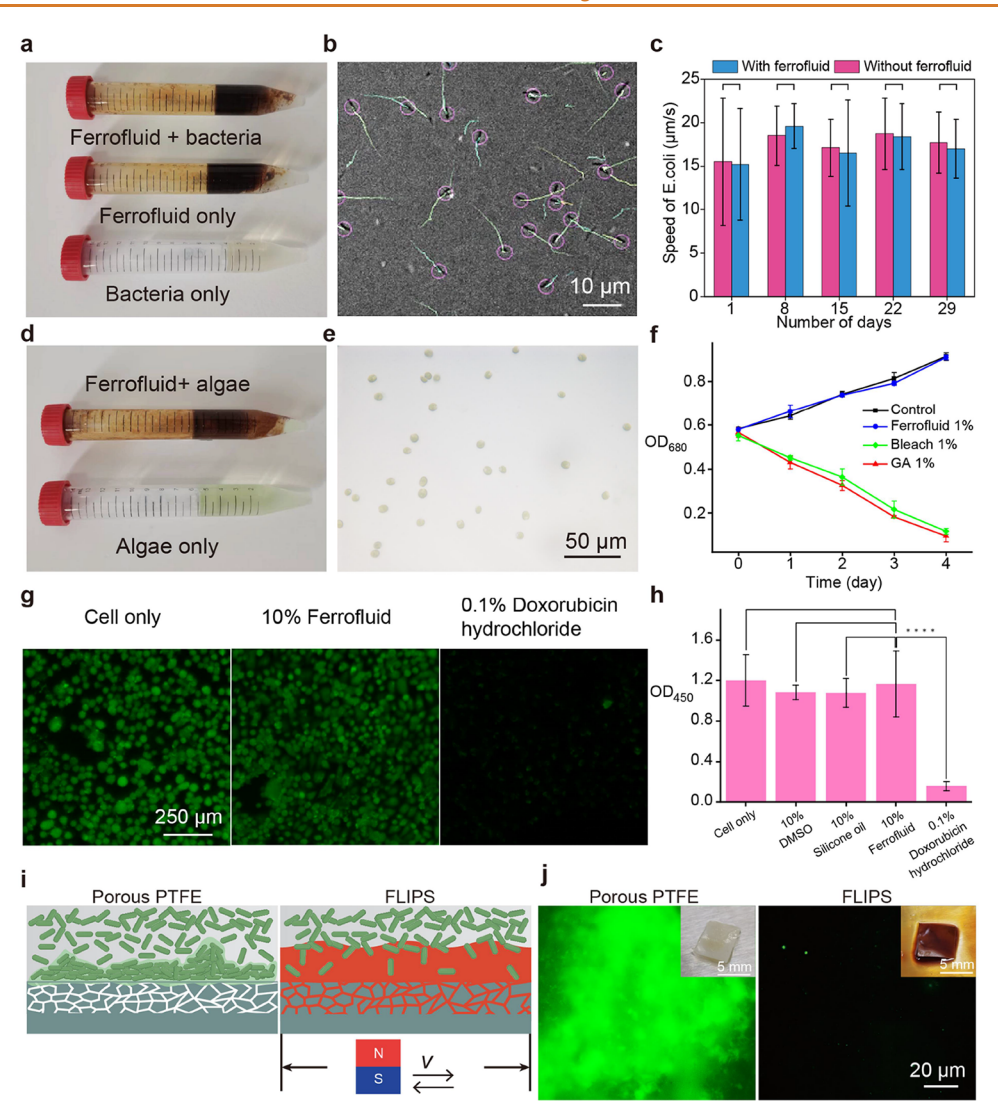


Figure 4. Bioinertness and antibiofouling properties of silicone oil-based ferrofluid. (a) Photo of centrifugal tubes containing ferrofluid and bacteria (*E. coli*), ferrofluid only, and bacteria only. (b) Representative microscope image of tracked bacteria motion after cultivation with silicone oil-based ferrofluid for 29 days. (c) Plots of speeds of bacteria with and without ferrofluids versus time. The error bars are the standard deviations of Gaussian fits of approximately 200 bacteria. Two sample *t* tests show no significant difference between the swimming speeds of the two groups. (d) Photos of centrifugal tubes containing ferrofluid and algae (*C. reinhardtii*) and algae only. (e) Representative image of algae under a light microscope after cultivation with silicone oil-based ferrofluid for 2 weeks. (f) Plots of optical densities at 680 nm versus time for an algae culture (control) and cultures with ferrofluid, bleach, and glutaraldehyde. The error bars are the standard deviations of absorptions of three samples. (g) Fluorescent images of live-stained HeLa cell-only culture, HeLa cell culture with 10% silicone oil-based ferrofluid, and HeLa cell culture with 0.1% doxorubicin hydrochloride. (h) Optical densities of cell-only cultures and HeLa cell cultures with 10% DMSO, 10% silicone oil-based ferrofluid, and 0.1% doxorubicin hydrochloride. The error bars are standard deviations of eight replicates. The stars indicate that the *p*-value of the two-sample *t* test is less than 0.0001. (i) Schemes of *P. aeruginosa* biofilm on porous PTFE film (left) and FLIPS (right). An oscillating magnetic field was applied via a magnet below the FLIPS. (j) Fluorescence images showing extensive *P. aeruginosa* biofilm attachment on porous PTFE (left) and no biofilm attachment on FLIPS (right) surfaces after 7 days. The insets are the corresponding photos of the control PTFE and FLIPS surfaces after 7 days of biofilm growth.

effects of any surface-active impurities that may cause errors. Second, the small positive value of S = 2.9 mN/m for the Krytox wrapping layer around a water droplet in the air leaves a small margin of error. A ~5% error in the measurement of the interfacial tension between Krytox and water could change the sign of S. The existence of a Krytox wrapping layer around the water in the air, however, is not in doubt: its existence prevents the complete wrapping of a water droplet by ferrofluid, as shown in the left image of Figure 3e.

To calculate the energy of Casimir—Lifshitz interactions (Supplementary Section S4.1), we used the refractive index and the first ionization potential to construct a model for imaginary

frequency susceptibility  $\varepsilon(i\xi)$  (Figure 3b). From the values of  $\varepsilon(i\xi)$ , we calculate the Hamaker coefficients and the interaction energy  $G_{132}$  versus the thin film thickness. Figure 3c,d shows the configurations in which the surrounding fluids are air and oleic acid, respectively. The principle of free energy minimization in equilibrium systems suggests that ferrofluid or Krytox wrapping layers in the air tend to grow thicker and, hence, are stable. In contrast, ferrofluid or Krytox wrapping layers in oleic acid tend to grow thinner and eventually disappear, and hence, they are unstable. These results agree with the experimental observations.

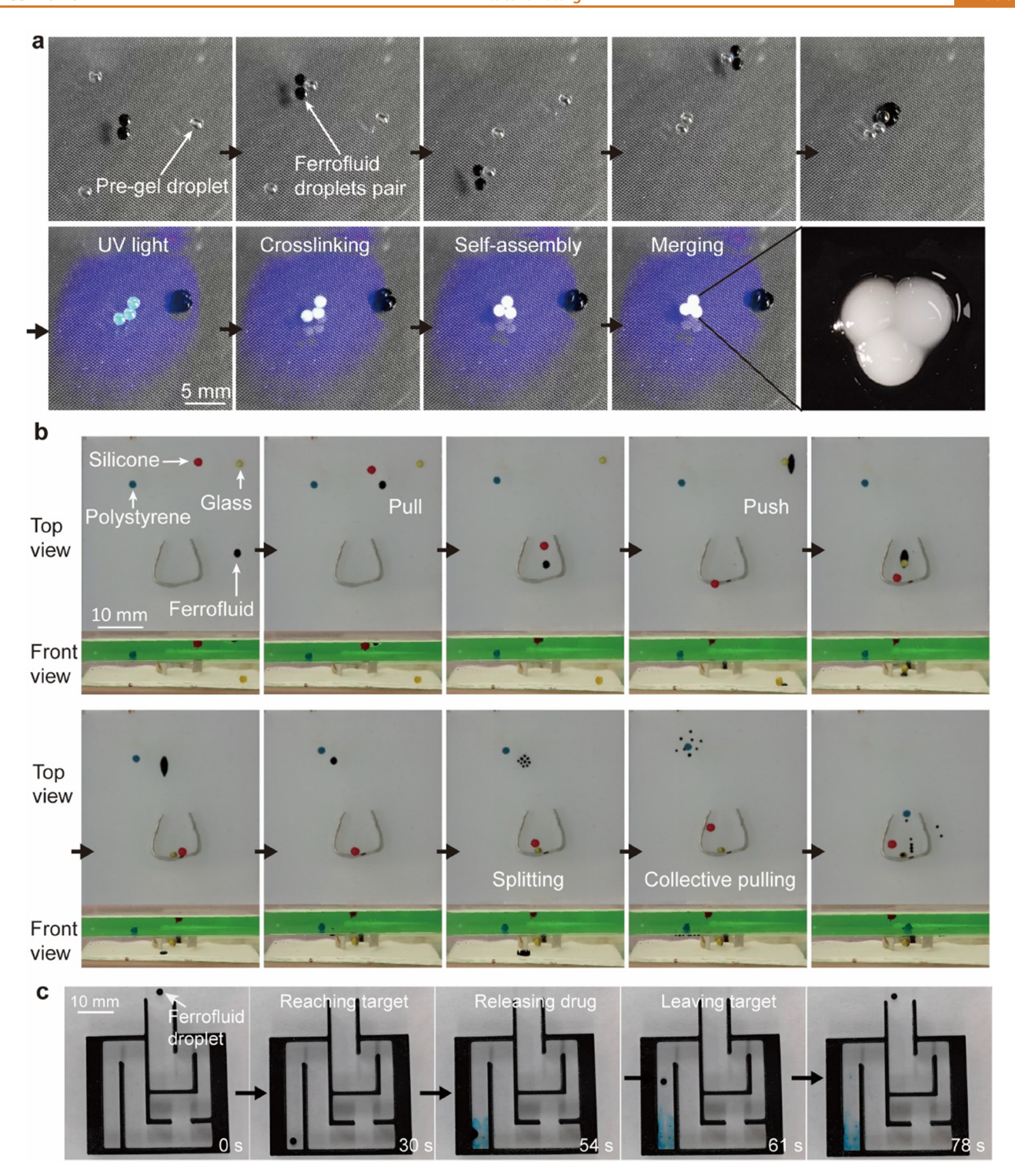


Figure 5. Manipulation of objects using droplets of ferrofluid in 2D and 3D. (a) Transport and self-assembly of three PNIPAM hydrogel droplets by controlling a pair of ferrofluid droplets. The assembled hydrogel droplet preserves partly the initial spherical shapes of the hydrogel droplets. (b) Transport of three particles at three interfaces to the target area in the U-shaped aluminum ring. The top and bottom liquids are water (dyed green) and a fluorocarbon liquid, respectively. The red silicone particle at the air—water interface is pulled into the target area. The yellow glass bead at the bottom is pushed into the target region. The blue polystyrene bead is pulled collectively by small ferrofluid droplets. (c) Demonstration of dye release from a ferrofluid droplet inside a maze.

We make two further comments about the calculation of the Casimir–Lifshitz interaction energy  $G_{132}$ . First, there are two simplified methods to calculate  $G_{132}^9$ : one based on combining relations (Supplementary Section S4.2 and Table S5) and one based on nonretarded Hamaker constants (Supplementary

Section S4.3 and Table S6). While the former gives the correct predictions, the latter gives mixed results. Combining relations uses interfacial tensions as input, so the accurate measurements of interfacial tensions in our experiments produced the correct results. On the other hand, the simplified method to calculate

nonretarded Hamaker constants assumes the same electronic absorption frequency of 3  $\times$  10<sup>15</sup> Hz (equivalent to a first ionization potential of 12.4 eV) for all media, <sup>64</sup> but this assumption introduces too much error, particularly for silicone oil, whose first ionization potential is 6.37 eV (Table S3), so this method produced mixed results. Second, our full calculation could be further improved by incorporating more terms into the models of imaginary frequency susceptibility  $\varepsilon(i\xi)$ . The benefit is that the results will be quantitatively accurate and enable us to design more intricate systems by balancing disjoining pressures (Figure S7) with magnetic and capillary pressures.

To demonstrate the potential of a silicone oil-based ferrofluid in magnetic digital microfluidics, we performed droplet-based chemical reactions on SLIPS (Figure 3g) and FLIPS (Figure 3h-j). On SLIPS, a robotic arm controlled the motion of a permanent magnet array, whose magnetic field gradient imposed a magnetic force on a ferrofluid droplet to move it. When the ferrofluid droplet was near a nonmagnetic droplet, it attracted the nonmagnetic droplet (basic aqueous solution of sodium hydroxide with a phenolphthalein indicator) via capillary interaction.<sup>65</sup> The two droplets became attached and moved together but were not mixed because of immiscible solvents. When another nonmagnetic droplet (aqueous solution of hydrochloric acid) was similarly attached, two aqueous droplets mixed, and the resulting acid-base reaction was monitored from the gradual color change (Movie S2). On FLIPS, three droplets of different volumes were mixed in a ferrofluid ring to perform the Griess test (Figure 3h and Movie S3). The Griess test can determine the concentration of nitrite in a solution and is widely used to detect urinary tract infections and bacteriuria. 66,67 A ring magnet was used to create a ferrofluid ring as a two-dimensional (2D) reaction vessel. This ferrofluid 2D reaction vessel opens automatically while moving to take in and mix droplets. Absorptions at 540 nm were measured for samples of different nitrite concentrations, and a linear dependence of absorption on nitrite concentration was obtained in the range of 1–100  $\mu$ M (Figures 3i,j). The strong linear dependence and the high sensitivity of the test indicate that silicone oil-based ferrofluid does not interact with any reagents in the test because of its chemical inertness.

The silicone oil-based ferrofluid is biologically inert. We verify its bioinertness in bacteria, algae, and mammalian cell cultures (Figure 4a-h). We cultured Escherichia coli in the presence of silicone oil-based ferrofluid for about a month and measured the swimming speeds of bacteria as an indicator of their viability (Figure 4a,b and Movie S4). The swimming speeds of bacteria in cultures with and without ferrofluid showed no statistically significant difference (Figure 4c). Similarly, we cultured Chlamydomonas reinhardtii in the presence of silicone oilbased ferrofluid and performed toxicity tests (Figures 4d-f and S8). The optical densities of the cultures with and without the ferrofluid show the same increase over a four-day period, indicating no influence of the ferrofluid on the algae growth, whereas the optical densities of cultures with common disinfectants bleach and glutaraldehyde show a marked decrease over the same period, as a result of the disinfectants' toxicity (Figure 4f).

Moreover, we cultured human HeLa cells in the presence of silicone oil-based ferrofluid and performed the in vitro cellular toxicity test according to ISO 10993-5 (Figure 4g, h). Fluorescent images taken after 24 h show no visual difference between the cell-only control group and the group with 10% ferrofluid. In contrast, most cells died in the negative control

group of 0.1% doxorubicin hydrochloride, a cytotoxic drug (Figures 4g and S9). To corroborate this result, Figure 4f shows the optical densities at 450 nm for the groups of cell-only, 10% DMSO, 10% silicone oil, and 10% ferrofluid showing similar absorbance after 24 h of incubation, indicating no influence of the ferrofluid on cell growth. In contrast, the optical density of the control group treated with 0.1% doxorubicin hydrochloride shows significantly low absorbance with p < 0.0001 (Figure 4f).

The response of ferrofluid to external magnetic fields allows us to engineer FLIPS with dynamic topography. Surfaces with active microscale topography have been shown to prevent biofilm formation. <sup>68</sup> We hypothesize that the dynamic topography of FLIPS could similarly prevent biofilm formation. To test this hypothesis, we cultured a common clinical pathogen *Pseudomonas aeruginosa* on FLIPS in the presence of an oscillating magnet for a week (Figure 4i). A control sample on a porous polytetrafluoroethylene (PTFE) membrane but without ferrofluid was also prepared. Fluorescent images taken after 7 days show significant biofilm accumulation on the control sample but no biofilm on the FLIPS sample (Figures 4j and S10). This result suggests the potential of the antibiofouling application of properly engineered dynamic FLIPS.

Soft Robots Based on Silicone Oil-Based Ferrofluid. Ferrofluid-based soft robots represent an emerging area of applications of ferrofluid. 15–17,19–23 The motivation is that liquids are easier to deform than elastic solids; and magnetic liquids, in particular, can be manipulated via external magnetic fields to navigate through narrow channels to reach occluded regions and perform tasks such as imaging, cargo delivery, or localized heating. The chemical and biological inertness of the new silicone oil-based ferrofluids suggests that they can be used to construct soft robots to manipulate particles of a variety of chemical compositions. As proof-of-concept demonstrations, we show the behaviors of droplet-based robots made of silicone oil-based ferrofluids in composite fluidic media environments consisting of water and a fluorocarbon fluid. This section demonstrates the use of millimeter-scale ferrofluid droplets to manipulate various particles.

Using silicone oil-based ferrofluids, we performed twodimensional (2D) manipulation of a silicone rubber ball, a gas bubble, and a water droplet, and the 2D assembly and crosslinking of three hydrogel pregel droplets at the interface of a fluorocarbon oil and air. The former (Figure S11 and Movie S5) is a simple demonstration to showcase the versatility of objects that the ferrofluid is capable of handling, while the latter (Figure 5a and Movie S6) involves slightly more complex robotic manipulation and timed rupture of wrapping layers. More specifically, the latter case (Figure 5a) involves the transport, self-assembly, and cross-linking of three droplets of poly(Nisopropylacrylamide) (PNIPAM) pregel solutions by a pair of ferrofluid droplets. Two parallel stacks of permanent magnets placed on the end effector of a robotic arm created a magnetic double-well potential and were used to trap a pair of ferrofluid droplets. This pair of ferrofluid droplets can attach a single droplet of pregel solution between them via capillary force to facilitate the transport of the pregel droplet. When pregel droplets were brought to proximity, they self-assembled via mutual capillary attraction to form a triangular configuration. UV light irradiation initiated the cross-linking reaction during the self-assembly process. Continued UV light irradiation facilitated the rupture of the fluorocarbon wrapping layer around the hydrogel droplets and the formation of a continuous piece of hydrogel that preserves the overall shape of the

triangular configuration. This hydrogel piece was shown to exhibit the usual thermal responsiveness of PNIPAM (Figure S12). We note that this simultaneous cross-linking and shape-preserving capability was only recently accomplished using droplets wrapped by expensive lipid molecules, <sup>69</sup> and our use of a fluorocarbon wrapping layer at the liquid—air interface to achieve the same capability opens doors to convenient fabrication of hydrogel network structures, with potential applications in smart multifunctional materials and biomedicine.

We further demonstrate the capability of silicone oil-based ferrofluid to manipulate particles in 3D in a solution containing a top water layer (dyed green) and a bottom fluorocarbon liquid layer (Figure 5b and Movie S7). A silicone rubber particle (red, density  $\sim 0.9 \text{ g/cm}^3$ ), a polystyrene particle (blue,  $\sim 1 \text{ g/cm}^3$ ), and a glass bead (yellow,  $\sim 2-3$  g/cm<sup>3</sup>) were positioned at the air-water interface, the water-fluorocarbon liquid interface, and the fluorocarbon liquid-container interface, respectively. The density of silicone oil-based ferrofluid (~1.3 g/cm<sup>3</sup>) is larger than water, but smaller than the fluorocarbon oil ( $\sim$ 1.9 g/cm<sup>3</sup>). The stable position of a ferrofluid droplet is at the waterfluorocarbon oil interface, but it can float at the air-water interface via a capillary force. We moved a ferrofluid droplet across these interfaces by changing the vertical distance of the permanent magnet with respect to the bottom of the container. Using the ferrofluid droplet as a manipulator, we pulled the silicone particle, pushed the glass bead, and pulled the polystyrene particle via the collective efforts of many smaller ferrofluid droplets at their respective interfaces toward a common area enclosed by a U-shaped aluminum strip. The formation of the smaller droplets takes advantage of the hysteresis of ferrofluid surface instability 70: we moved the magnet close to the bottom of the container to induce surface instability and split the initial droplet into smaller droplets, and then moved away from the container so that the smaller droplets floated up to the water-fluorocarbon liquid interface and performed the transport task collectively. Overall, this demonstration showcases a variety of manipulation strategies based on the interplay among magnetic forces, buoyance forces, and capillary interactions. It promises great flexibility in the future design of soft robots based on silicone oil-based ferrofluid.

To demonstrate the potential of silicone oil-based ferrofluid for drug delivery, we encapsulated a water-soluble dye in a ferrofluid droplet and delivered the dye inside a maze (Figure 5c and Movie S8). Permanent magnets below the maze controlled the movement and deformation of the ferrofluid droplet. In water, the ferrofluid droplet maintained a nearly spherical shape. Moving the permanent magnets horizontally rolled the droplet with little resistance. Moving the permanent magnets vertically closer to the maze increased the magnetic field's strength, deformed the droplet, and released the dye. After the release, the permanent magnets retracted to decrease the magnetic field's strength, and the droplet became spherical again and could be rolled to exit the maze. This demonstration shows the navigation of a ferrofluid droplet inside a complex channel and drug release through simple magnetic field control and suggests the potential of the silicone oil-based ferrofluid as a drug carrier.

# **CONCLUSIONS**

We have reported the facile synthesis of a silicone oil-based ferrofluid that displays the characteristic surface instability of high-quality ferrofluid. This high-quality silicone oil-based ferrofluid has allowed us to construct various smart multifunctional interfacial materials and soft robots.

This report raises a few immediate questions that warrant further investigations. First, further optimization and systematic exploration of the synthetic conditions, particularly with automated laboratory hardware, will benefit mechanistic studies and efforts to scale up the synthesis for potential commercial applications. Second, the ability to modify the side chains in polyalkylsiloxane affords us the capability to fine-tune Casimir—Lifshitz interactions of ferrofluid with other liquids; quantifying these interactions will require more detailed models of imaginary frequency susceptibility  $\varepsilon(i\xi)$ ; the parameters for these models may be obtained from direct absorption measurements. Third, the dynamic interface between magnetically actuated silicone oil-based ferrofluids and aqueous solutions of micro-organisms needs to be examined in detail.

Finally, we stress that the wholistic perspective of the entire process from synthesis to the characterization of structures and properties, and to the exploration of functions allows us to tailor the synthesis—such as nanoparticle composition and sizes, the types of monocarboxyl-terminated siloxanes, and the types of silicone oils—for specific applications. We envision that our silicone oil-based ferrofluid may find applications in artificial muscle, <sup>71</sup> low-temperature active fluids, <sup>31</sup> microscopic thermal management systems <sup>72</sup> or sensors, <sup>28</sup> thrumbus removal, <sup>73</sup> and targeted tumor therapy. <sup>74</sup>

#### **METHODS**

Materials. Ferric chloride hexahydrate was obtained from Sigma-Aldrich. Dimethylsilicone oil, ammonia, ferrous sulfate heptahydrate, nhexane, oleic acid, grape seed oil phosphate-buffered saline (PBS), and glutaraldehyde were obtained from Macklin. Monocarboxydecyl terminated polydimethylsiloxane MCR-B12 (PDMS-C<sub>10</sub>COOH) was obtained from Gelest. N-Isopropylacrylamide (NIPAm) was obtained from Adamas. N,N'-Methylenebis(acrylamide) (MBA) was obtained from Aladdin, and  $\alpha$ -ketoglutaric acid ( $\alpha$ -KGA) was obtained from Amethyst. Polytetrafluoroethylene (PTFE) membranes with an average pore size of 10  $\mu$ m were obtained from Sterlitech and used as received. The perfluoropolyether oil used for instabilities and wrapping was Dupont Krytox GPL 100, obtained from 3 M. Perfluoropolyether for hydrogel manipulation was obtained from Macklin (Mw = 4500). FC3283 for the manipulation of ferrofluid microdroplet swarms was obtained from 3M. Griess Reagent Kit for Nitrite Determination G-7921 was obtained from Invitrogen. Cell Apoptosis Detection Kit with SYTOX Green, Cell Counting Kit-8, and Calcein/PI Cell Viability/ Cytotoxicity Assay Kit were obtained from Beyotime. PBST (PBS with 0.05% Tween20, Ca<sup>2+</sup>, and Mg<sup>2+</sup>, pH 7.4, 0.01M) was obtained from ACMEC. Escherichia coli and Pseudomonas aeruginosa were purchased from BeNa Culture Collection Biological Technology Co., Ltd. Chlamydomonas reinhardtii was purchased from Shanghai Guangyu Biological Technology Co., Ltd. Adriamycin hydrochloride, DMSO, THF, Acetonitrile, ethyl acetate, dichloromethane, concentrated phosphoric acid, sulfuric acid, and hydrochloric acid were obtained from Adamas-Life.

**Synthesis.** In typical syntheses, ferric chloride hexahydrate solution (0.1-0.5 mol/L) and ferrous sulfate heptahydrate solution (0.05-0.25 mol/L) were mixed in a three-neck round-bottom flask containing deionized water (100 mL), and then, two drops of concentrated sulfuric acid solution were added. The flask was placed in an ultrasonic bath, and the water temperature was set at  $50\,^{\circ}\text{C}$ . An overhead mechanical stir blade was inserted via the middle opening of the flask, and the rotational speed was set at 200 rpm. The ratio of  $\text{Fe}^{3+}\text{:Fe}^{2+}$  ions was 1.5-2.5:1. The solution was stirred for 5-10 min. Then the ultrasonication was turned on (nominal power: 180 W, nominal frequency: 40 kHz; measured power density:  $\sim 0.7 \text{ W/cm}^2$ , measured frequency:  $\sim 30 \text{ kHz}$ ). 10-20 mL of ammonia was measured with a graduated cylinder and added from the side neck of the flask all at once. The mixture turned black while being stirred continuously. Immediately after the addition of ammonia, 3-7 g of PDMS-

ACS Nano www.acsnano.org Article

C<sub>10</sub>COOH was added to the mixture via another side neck of the flask all at once. The estimated molar ratios of ingredients are as follows:  ${\rm Fe^{3+}:Fe^{2+}:OH^-:PDMS-C_{10}COOH}=3-5:2:16-24:1.$  The ultrasonic was kept on, and the stirring was continued for 0.5 h at 50 °C. During the coprecipitation and surface functionalization, except when reagents were added, the side openings of the three-neck flask were blocked with glass stoppers. After the stirring was stopped, the black precipitate was sedimented using a permanent magnet and washed with acetone several times. Afterward, *n*-hexane (6–8 mL) was added to the black precipitate to redisperse the functionalized nanoparticles. The dispersion was kept in an ultrasonic bath at 50 °C for 5–10 min to remove traces of acetone and ammonia. Finally, dimethylsilicone oil (2–6 mL) was added to the dispersion, and the *n*-hexane was removed by heating at 80–90 °C in an ultrasonic bath.

Other experimental procedures are included in the Methods section of the Supporting Information file.

#### **ASSOCIATED CONTENT**

# Supporting Information

The Supporting Information is available free of charge at https://pubs.acs.org/doi/10.1021/acsnano.4c16689.

Additional experimental details and theoretical calculations related to polymer mixing, M-H curves, and the stabilities of wrapping layers; reported synthesis of silicone oil-based ferrofluids (Table S1); commercial silicone oil-based ferrofluids (Table S2); physical properties of liquids (Tables S3 and S4); results of calculations related to stabilities of thin films (Tables S5 and S6); results of the control experiments for the synthesis (Figure S1); NMR and GPC characterization of surfactant stability (Figures S2 and S3); ferrofluid stability test (Figure S4); TEM analysis of nanoparticles (Figure S5); images of pendant drops (Figure S6); additional images of wrapping layers (Figure S7); additional data on biocompatibility (Figures S8-S10); manipulation of various objects (Figure S11); and thermal response of hydrogel (Figure S12) (PDF)

Wrapping and unwrapping of a ferrofluid layer around a water droplet (MP4)

Droplet-based acid—base reaction monitored by color change using a ferrofluid droplet on SLIPS (MP4)

Mixing and shaking with the ferrofluid ring on FLIPS (MP4)

Speed tracking of bacteria with and without the ferrofluid (MP4)

Manipulation of a silicone rubber ball, an air bubble, and a water droplet at the interface of a fluorocarbon oil and the air (MP4)

2D assembly and cross-linking of three hydrogel pregel droplets (MP4)

Manipulation of particles at three interfaces via 3D motion of a ferrofluid droplet (MP4)

Demonstration of dye release from a ferrofluid microrobot (MP4)

## **AUTHOR INFORMATION**

# **Corresponding Author**

Wendong Wang — University of Michigan—Shanghai Jiao Tong University Joint Institute, Shanghai Jiao Tong University, Shanghai 200240, China; National Key Laboratory of Advanced Micro and Nano Manufacture Technology, Shanghai Jiao Tong University, Shanghai 200240, China; orcid.org/0000-0003-3007-1750;

Email: wendong.wang@sjtu.edu.cn

#### **Authors**

Leilei Chen – University of Michigan–Shanghai Jiao Tong University Joint Institute, Shanghai Jiao Tong University, Shanghai 200240, China

Hengao Yu — University of Michigan—Shanghai Jiao Tong University Joint Institute, Shanghai Jiao Tong University, Shanghai 200240, China

Jilan Yang — University of Michigan—Shanghai Jiao Tong University Joint Institute, Shanghai Jiao Tong University, Shanghai 200240, China; Present Address: School of Engineering, Shanghai Sanda University, Shanghai 201209, China

Jinzhuo Shi – University of Michigan–Shanghai Jiao Tong University Joint Institute, Shanghai Jiao Tong University, Shanghai 200240, China

Chun-he Li — University of Michigan—Shanghai Jiao Tong University Joint Institute, Shanghai Jiao Tong University, Shanghai 200240, China

**Zijie** Qu – University of Michigan–Shanghai Jiao Tong University Joint Institute, Shanghai Jiao Tong University, Shanghai 200240, China

Complete contact information is available at: https://pubs.acs.org/10.1021/acsnano.4c16689

# **Author Contributions**

L.C. and H.Y. contributed equally to this work. W.W., L.C., H.Y., and designed the research. L.C. performed the experiments on the ferrofluid droplets' surface instability, droplet manipulation, and wrapping-layer-related calculations. L.C. and J.Y. performed the synthesis of the ferrofluids, L.C. and J.S. performed the interfacial properties and functions, L.C. and C.L. performed the bioinertness and antibiofouling properties, H.Y. performed the preparation of pregel solutions and microdroplet. L.C., H.Y., and W.W. wrote the manuscript. All authors edited the manuscript. W.W. and Z.Q. supervised the research and acquired the funding.

#### **Funding**

This work was supported by the National Natural Science Foundation of China (project number 22175115), the Science and Technology Commission of Shanghai Municipality (project number 23ZR1433700), and the UM-SJTU JI start-up fund.

#### Notes

The authors declare the following competing financial interest(s): One Chinese patent based on this work has been filed.

# **ACKNOWLEDGMENTS**

W.W. thanks Dr. J. Timonen for helpful discussions. L.C. thanks Mr. Ligang Zhou from the Instrumental Analysis Center of Shanghai Jiao Tong University for providing testing support, Ms. Xiaoli Bao from the Biosafety Laboratory for her experimental guidance, Dr. Yuan and Dr. Nie from Laboratory Animal Center for their help with HeLa cell experiments. We thank Dr. M. Dong for his assistance in rheological measurements.

#### **REFERENCES**

- (1) Rosensweig, R. E. Ferrohydrodynamics; Dover Publications: Mineola, N.Y., 1997.
- (2) Ferrofluids: Magnetically Controllable Fluids and Their Applications; Odenbach, S., Ed.; Lecture notes in physics; Springer: Berlin; New York, 2002.

- (3) Torres-Díaz, I.; Rinaldi, C. Recent Progress in Ferrofluids Research: Novel Applications of Magnetically Controllable and Tunable Fluids. *Soft Matter* **2014**, *10* (43), 8584–8602.
- (4) Zhang, X.; Sun, L.; Yu, Y.; Zhao, Y. Flexible Ferrofluids: Design and Applications. *Adv. Mater.* **2019**, *31* (51), No. 1903497.
- (5) Socoliuc, V.; Avdeev, M. V.; Kuncser, V.; Turcu, R.; Tombácz, E.; Vékás, L. Ferrofluids and Bio-Ferrofluids: Looking Back and Stepping Forward. *Nanoscale* **2022**, *14* (13), 4786–4886.
- (6) Dassisti, M.; Brunetti, G. Introduction to Magnetorheological Fluids. In *Encyclopedia of Smart Materials*; Elsevier: 2021; pp 187–202.
- (7) Colloidal Magnetic Fluids: Basics, Development, and Application of Ferrofluids; Odenbach, S., Ed.; Lecture notes in physics; Springer Verlag: Berlin, 2009.
- (8) Kole, M.; Khandekar, S. Engineering Applications of Ferrofluids: A Review. J. Magn. Magn. Mater. 2021, 537, No. 168222.
- (9) Wang, W.; Timonen, J. V. I.; Carlson, A.; Drotlef, D.-M.; Zhang, C. T.; Kolle, S.; Grinthal, A.; Wong, T.-S.; Hatton, B.; Kang, S. H.; Kennedy, S.; Chi, J.; Blough, R. T.; Sitti, M.; Mahadevan, L.; Aizenberg, J. Multifunctional Ferrofluid-Infused Surfaces with Reconfigurable Multiscale Topography. *Nature* **2018**, 559 (7712), 77–82.
- (10) Dunne, P.; Adachi, T.; Dev, A. A.; Sorrenti, A.; Giacchetti, L.; Bonnin, A.; Bourdon, C.; Mangin, P. H.; Coey, J. M. D.; Doudin, B.; Hermans, T. M. Liquid Flow and Control without Solid Walls. *Nature* **2020**, *581* (7806), *58*–62.
- (11) Zhang, J.; Wang, X.; Wang, Z.; Pan, S.; Yi, B.; Ai, L.; Gao, J.; Mugele, F.; Yao, X. Wetting Ridge Assisted Programmed Magnetic Actuation of Droplets on Ferrofluid-Infused Surface. *Nat. Commun.* **2021**, *12* (1), 7136.
- (12) Lin, H.; Yu, W.; Sabet, K. A.; Bogumil, M.; Zhao, Y.; Hambalek, J.; Lin, S.; Chandrasekaran, S.; Garner, O.; Di Carlo, D.; Emaminejad, S. Ferrobotic Swarms Enable Accessible and Adaptable Automated Viral Testing. *Nature* **2022**, *611* (7936), 570–577.
- (13) Yu, W.; Lin, H.; Wang, Y.; He, X.; Chen, N.; Sun, K.; Lo, D.; Cheng, B.; Yeung, C.; Tan, J.; Di Carlo, D.; Emaminejad, S. A Ferrobotic System for Automated Microfluidic Logistics. *Science*. *Robotics* **2020**, *5* (39), No. eaba4411.
- (14) Nasirimarekani, V.; Benito-Lopez, F.; Basabe-Desmonts, L. Tunable Superparamagnetic Ring (tSPRing) for Droplet Manipulation. *Adv. Funct Materials* **2021**, *31* (32), No. 2100178.
- (15) Fan, X.; Dong, X.; Karacakol, A. C.; Xie, H.; Sitti, M. Reconfigurable Multifunctional Ferrofluid Droplet Robots. *Proc. Natl. Acad. Sci. U.S.A.* **2020**, *117* (45), 27916–27926.
- (16) Sun, M.; Fan, X.; Tian, C.; Yang, M.; Sun, L.; Xie, H. Swarming Microdroplets to a Dexterous Micromanipulator. *Adv. Funct Materials* **2021**, *31* (19), No. 2011193.
- (17) Cenev, Z.; Harischandra, P. A. D.; Nurmi, S.; Latikka, M.; Hynninen, V.; Ras, R.; Timonen, J.; Zhou, Q. Ferrofluidic Manipulator: Automatic Manipulation of Nonmagnetic Microparticles at the Air–Ferrofluid Interface. *IEEE/ASME Trans. Mechatron.* **2021**, *26* (4), 1932–1940.
- (18) Ahmed, R.; Ilami, M.; Bant, J.; Beigzadeh, B.; Marvi, H. A Shapeshifting Ferrofluidic Robot. *Soft Robotics* **2021**, *8* (6), 687–698.
- (19) Sun, M.; Hao, B.; Yang, S.; Wang, X.; Majidi, C.; Zhang, L. Exploiting Ferrofluidic Wetting for Miniature Soft Machines. *Nat. Commun.* **2022**, *13* (1), 7919.
- (20) Fan, X.; Jiang, Y.; Li, M.; Zhang, Y.; Tian, C.; Mao, L.; Xie, H.; Sun, L.; Yang, Z.; Sitti, M. Scale-Reconfigurable Miniature Ferrofluidic Robots for Negotiating Sharply Variable Spaces. *Sci. Adv.* **2022**, *8* (37), No. eabq1677.
- (21) Sun, M.; Yang, S.; Jiang, J.; Zhang, L. Horizontal and Vertical Coalescent Microrobotic Collectives Using Ferrofluid Droplets. *Adv. Mater.* **2023**, *35*, No. 2300521.
- (22) Cenev, Z. M.; Havu, V.; Timonen, J. V. I.; Zhou, Q. Ferrofluidic Manipulator: Theoretical Model for Single-Particle Velocity. *IEEE/ASME Trans. Mechatron.* **2023**, 28, 2679–2689.
- (23) Yang, L.; Sun, M.; Zhang, M.; Zhang, L. Multimodal Motion Control of Soft Ferrofluid Robot With Environment and Task Adaptability. *IEEE/ASME Trans. Mechatron.* **2023**, 28, 3099–3109.

- (24) Ahmed, R.; Calandra, R.; Marvi, H. Learning to Control a Three-Dimensional Ferrofluidic Robot. *Soft Robot.* **2023**, *11*, 5.
- (25) Chen, J.; Xia, L.; Wu, X.; Du, L.; Liu, R.; Liu, J.; Li, X.; Sun, Y.; Colvin, V. L.; Cao, Q. The Exploration of Multifunctional Liquid Robotics with Ferrofluids: Fabrication, Control, Operation and Sensing. *Nano Energy* **2024**, *131*, No. 110169.
- (26) Yu, H.; Fu, Y.; Zhang, X.; Chen, L.; Qi, D.; Shi, J.; Wang, W. Programmable Active Matter across Scales. *Program. mater.* **2023**, *1*, No. e7.
- (27) Kaspar, C.; Ravoo, B. J.; van der Wiel, W. G.; Wegner, S. V.; Pernice, W. H. P. The Rise of Intelligent Matter. *Nature* **2021**, *594* (7863), 345–355.
- (28) Serwane, F.; Mongera, A.; Rowghanian, P.; Kealhofer, D. A.; Lucio, A. A.; Hockenbery, Z. M.; Campàs, O. In Vivo Quantification of Spatially Varying Mechanical Properties in Developing Tissues. *Nat. Methods* **2017**, *14* (2), 181–186.
- (29) Lohmann, R.; Cousins, I. T.; DeWitt, J. C.; Glüge, J.; Goldenman, G.; Herzke, D.; Lindstrom, A. B.; Miller, M. F.; Ng, C. A.; Patton, S.; Scheringer, M.; Trier, X.; Wang, Z. Are Fluoropolymers Really of Low Concern for Human and Environmental Health and Separate from Other PFAS? *Environ. Sci. Technol.* **2020**, *54* (20), 12820–12828.
- (30) Brydson, J. A. Silicones and Other Heat-Resisting Polymers. In *Plastics Materials*; Elsevier: 1989; pp 763–800.
- (31) Moretto, H.; Schulze, M.; Wagner, G. Silicones. In *Ullmann's Encyclopedia of Industrial Chemistry*; Wiley-VCH: 2000.
- (32) Mazurek, M. H. Silicones. In Comprehensive Organometallic Chemistry III; Elsevier: 2007; pp 651–697.
- (33) Aziz, T.; Fan, H.; Khan, F. U.; Haroon, M.; Cheng, L. Modified Silicone Oil Types, Mechanical Properties and Applications. *Polym. Bull.* **2019**, *76* (4), 2129–2145.
- (34) Duraivel, S.; Laurent, D.; Rajon, D. A.; Scheutz, G. M.; Shetty, A. M.; Sumerlin, B. S.; Banks, S. A.; Bova, F. J.; Angelini, T. E. A Silicone-Based Support Material Eliminates Interfacial Instabilities in 3D Silicone Printing. *Science* **2023**, 379 (6638), 1248–1252.
- (35) Howell, C.; Grinthal, A.; Sunny, S.; Aizenberg, M.; Aizenberg, J. Designing Liquid-Infused Surfaces for Medical Applications: A Review. *Adv. Mater.* **2018**, *30* (50), No. 1802724.
- (36) Amini, S.; Kolle, S.; Petrone, L.; Ahanotu, O.; Sunny, S.; Sutanto, C. N.; Hoon, S.; Cohen, L.; Weaver, J. C.; Aizenberg, J.; Vogel, N.; Miserez, A. Preventing Mussel Adhesion Using Lubricant-Infused Materials. *Science* **2017**, 357 (6352), 668–673.
- (37) Krayukhina, E.; Tsumoto, K.; Uchiyama, S.; Fukui, K. Effects of Syringe Material and Silicone Oil Lubrication on the Stability of Pharmaceutical Proteins. *J. Pharm. Sci.* **2015**, *104* (2), 527–535.
- (38) Ludwig, D. B.; Carpenter, J. F.; Hamel, J.; Randolph, T. W. Protein Adsorption and Excipient Effects on Kinetic Stability of Silicone Oil Emulsions. *J. Pharm. Sci.* **2010**, *99* (4), 1721–1733.
- (39) Barca, F.; Caporossi, T.; Rizzo, S. Silicone Oil: Different Physical Proprieties and Clinical Applications. *BioMed. Research International* **2014**, 2014, 1–7.
- (40) Ichhpujani, P.; Jindal, A.; Jay Katz, L. Silicone Oil Induced Glaucoma: A Review. *Graefes Arch Clin Exp Ophthalmol* **2009**, 247 (12), 1585–1593.
- (41) Chagnon, M. S. Stable Ferrofluid Compositions and Method of Making Same. US4356098A, 1982.
- (42) Raj, K.; Rosensweig, R. E.; Aziz, L. M. Stable Polysiloxane Ferrofluid Compositions and Method of Making Same. US5851416A, 1998.
- (43) Dailey, J. P.; Phillips, J. P.; Li, C.; Riffle, J. S. Synthesis of Silicone Magnetic Fluid for Use in Eye Surgery. *J. Magn. Magn. Mater.* **1999**, *194* (1–3), 140–148.
- (44) Borduz, L.; Tsuda, S.; Hirota, Y. Ferrofluid Composition and Process. US6277298B1, 2001.
- (45) Wilson, K. S.; Goff, J. D.; Riffle, J. S.; Harris, L. A.; St Pierre, T. G. Polydimethylsiloxane-magnetite Nanoparticle Complexes and Dispersions in Polysiloxane Carrier Fluids. *Polymers for Advanced Techs* **2005**, *16* (2–3), 200–211.

- (46) Chen, H. J.; Wang, Y. M.; Qu, J. M.; Hong, R. Y.; Li, H. Z. Preparation and Characterization of Silicon Oil Based Ferrofluid. *Appl. Surf. Sci.* **2011**, 257 (24), 10802–10807.
- (47) Kim, J.-H.; Park, K.-B.; Kim, K.-S. Preparation and Characterization of Silicone and Fluorine-Oil-Based Ferrofluids. *Composites Research* **2017**, 30 (1), 41–45.
- (48) Zheng, H.; Shao, H.-P.; Lin, T.; Zhao, Z.-F.; Guo, Z.-M. Preparation and Characterization of Silicone-Oil-Based  $\gamma$ -Fe2O3Magnetic Fluid. *Rare Met.* **2018**, *37* (9), 803–807.
- (49) Zhou, Q.; Chen, F.; Liu, Y.; Li, J. Preparation and Stability Study of Carboxyl Terminated Silicone Oil Modified Silicone-Oil-Based Ferrofluid. *JMAG* **2019**, *24* (1), 49–56.
- (50) Li, L.; Li, D.; Wang, L.; Liang, Z.; Zhang, Z. Stable Silicone Oil Based Ferrofluids with Well Low-Temperature Fluidity Applied to Magnetic Fluid Seal. *J. Magn. Magn. Mater.* **2023**, *584*, No. 171077.
- (51) Mason, T. J.; Lorimer, J. P. Applied Sonochemistry: The Uses of Power Ultrasound in Chemistry and Processing; Wiley-VCH: Weinheim, 2001
- (52) Gedanken, A.; Perelshtein, I. Power Ultrasound for the Production of Nanomaterials. In *Power Ultrasonics*; Elsevier: 2015; pp 543–576
- (53) Martínez, R. F.; Cravotto, G.; Cintas, P. Organic Sonochemistry: A Chemist's Timely Perspective on Mechanisms and Reactivity. *J. Org. Chem.* **2021**, *86* (20), 13833–13856.
- (54) Lee, J. N.; Park, C.; Whitesides, G. M. Solvent Compatibility of Poly(Dimethylsiloxane)-Based Microfluidic Devices. *Anal. Chem.* **2003**, 75 (23), 6544–6554.
- (55) Rubinstein, M.; Colby, R. H. *Polymer Physics*; Oxford University Press: Oxford; New York, 2003.
- (56) Chantrell, R.; Popplewell, J.; Charles, S. Measurements of Particle Size Distribution Parameters in Ferrofluids. *IEEE Trans. Magn.* **1978**, *14* (5), 975–977.
- (57) Wong, T.-S.; Kang, S. H.; Tang, S. K. Y.; Smythe, E. J.; Hatton, B. D.; Grinthal, A.; Aizenberg, J. Bioinspired Self-Repairing Slippery Surfaces with Pressure-Stable Omniphobicity. *Nature* **2011**, 477 (7365), 443–447.
- (58) Lafuma, A.; Quéré, D. Slippery Pre-Suffused Surfaces. EPL 2011, 96 (5), 56001.
- (59) Smith, J. D.; Dhiman, R.; Anand, S.; Reza-Garduno, E.; Cohen, R. E.; McKinley, G. H.; Varanasi, K. K. Droplet Mobility on Lubricant-Impregnated Surfaces. *Soft Matter* **2013**, *9* (6), 1772–1780.
- (60) Schellenberger, F.; Xie, J.; Encinas, N.; Hardy, A.; Klapper, M.; Papadopoulos, P.; Butt, H.-J.; Vollmer, D. Direct Observation of Drops on Slippery Lubricant-Infused Surfaces. *Soft Matter* **2015**, *11* (38), 7617–7626.
- (61) Daniel, D.; Timonen, J. V. I.; Li, R.; Velling, S. J.; Aizenberg, J. Oleoplaning Droplets on Lubricated Surfaces. *Nature Phys.* **2017**, *13* (10), 1020–1025.
- (62) Parsegian, V. A. Van Der Waals Forces: A Handbook for Biologists, Chemists, Engineers, and Physicists; Cambridge University Press: New York, 2006.
- (63) Munday, J. N.; Capasso, F.; Parsegian, V. A. Measured Long-Range Repulsive Casimir–Lifshitz Forces. *Nature* **2009**, *457* (7226), 170–173.
- (64) Israelachvili, J. N. Intermolecular and Surface Forces, 3rd ed.; Academic Press: Burlington, MA, 2011.
- (65) Xu, H.; Zhou, Y.; Daniel, D.; Herzog, J.; Wang, X.; Sick, V.; Adera, S. Droplet Attraction and Coalescence Mechanism on Textured Oil-Impregnated Surfaces. *Nat. Commun.* **2023**, *14* (1), 4901.
- (66) Moorcroft, M. Detection and Determination of Nitrate and Nitrite: A Review. *Talanta* **2001**, *54* (5), 785–803.
- (67) Jungreis, E. SPOT TESTS. In *Encyclopedia of Analytical Science*; Elsevier: 2005; pp 383–400.
- (68) Gu, H.; Lee, S. W.; Carnicelli, J.; Zhang, T.; Ren, D. Magnetically Driven Active Topography for Long-Term Biofilm Control. *Nat. Commun.* **2020**, *11* (1), 2211.
- (69) Downs, F. G.; Lunn, D. J.; Booth, M. J.; Sauer, J. B.; Ramsay, W. J.; Klemperer, R. G.; Hawker, C. J.; Bayley, H. Multi-Responsive

- Hydrogel Structures from Patterned Droplet Networks. *Nat. Chem.* **2020**, *12* (4), 363–371.
- (70) Timonen, J. V. I.; Latikka, M.; Leibler, L.; Ras, R. H. A.; Ikkala, O. Switchable Static and Dynamic Self-Assembly of Magnetic Droplets on Superhydrophobic Surfaces. *Science* **2013**, *341* (6143), 253–257.
- (71) Kim, I. H.; Choi, S.; Lee, J.; Jung, J.; Yeo, J.; Kim, J. T.; Ryu, S.; Ahn, S.; Kang, J.; Poulin, P.; Kim, S. O. Human-Muscle-Inspired Single Fibre Actuator with Reversible Percolation. *Nat. Nanotechnol.* **2022**, *17* (11), 1198–1205.
- (72) Rosensweig, R. E. Heating Magnetic Fluid with Alternating Magnetic Field. J. Magn. Magn. Mater. 2002, 252, 370–374.
- (73) Li, Z.; Zhang, S.; Wang, Q.; Xu, Y.; Li, Y.; Chen, X.; Chen, P.; Chen, D.; Shi, Y.; Su, B. Untethered & Stiffness-Tunable Ferromagnetic Liquid Robots for Cleaning Thrombus in Complex Blood Vessels. *Adv. Mater.* **2024**, *36* (46), No. 2409142.
- (74) Ji, Y.; Bai, X.; Sun, H.; Wang, L.; Xu, J.; Gan, C.; Dai, Y.; Hui, H.; Feng, L. Biocompatible Ferrofluid Robot With Photothermal Property for Targeted Tumor Therapy. *IEEE Robot. Autom. Lett.* **2022**, 7 (4), 11517–11522.



CAS BIOFINDER DISCOVERY PLATFORM™

# CAS BIOFINDER HELPS YOU FIND YOUR NEXT BREAKTHROUGH FASTER

Navigate pathways, targets, and diseases with precision

**Explore CAS BioFinder** 

